Mineralogical Magazine, February 2010, Vol. 74(1), pp. 159–177

The structure of charoite, $(K,Sr,Ba,Mn)_{15-16}(Ca,Na)_{32}[(Si_{70}(O,OH)_{180})](OH,F)_{4.0}\cdot nH_2O$, solved by conventional and automated electron diffraction

I. Rozhdestvenskaya[1,2,*], E. Mugnaioli[3], M. Czank[2], W. Depmeier[2], U. Kolb[3], A. Reinholdt[4] and T. Weirich[4]

[1] Department of Crystallography, Geological Faculty, Saint Petersburg State University, University emb. 7/9, St. Petersburg, 199034, Russia
[2] Department of Crystallography, Institute of Geowissenschaften, Christian-Albrechts-University, Olshausenstrasse 40, D-24098, Kiel, Germany
[3] Institute of Physical Chemistry, Johannes Gutenberg-University, Welderweg 11, D-55099, Mainz, Germany
[4] Rheinisch-Westfaelische Technische Hochschule, Central Facility for Electron Microscopy, Aachen University, Ahornstrasse 55, D-52074, Aachen, Germany

[*Received 11 July 2009; Accepted 25 February 2010*]

ABSTRACT

Charoite, ideally $(K,Sr,Ba,Mn)_{15-16}(Ca,Na)_{32}[(Si_{70}(O,OH)_{180})](OH,F)_{4.0}\cdot nH_2O$, a rare mineral from the Murun massif in Yakutiya, Russia, was studied using high-resolution transmission electron microscopy, selected-area electron diffraction, X-ray spectroscopy, precession electron diffraction and the newly developed technique of automated electron-diffraction tomography. The structure of charoite (a = 31.96(6) Å, b = 19.64(4) Å, c = 7.09(1) Å, β = 90.0(1)º, V = 4450(24) Å^3, space group $P2_1/m$) was solved *ab initio* by direct methods from 2878 unique observed reflections and refined to R_1/wR_2 = 0.17/0.21. The structure can be visualized as being composed of three different dreier silicate chains: a double dreier chain, $[Si_6O_{17}]^{10-}$; a tubular loop-branched dreier triple chain, $[Si_{12}O_{30}]^{12-}$; and a tubular hybrid dreier quadruple chain, $[Si_{17}O_{43}]^{18-}$. The silicate chains occur between ribbons of edge-sharing Ca and Na-octahedra. The chains of tetrahedra and the ribbons of octahedra extend parallel to the z axis. K^+, Ba^{2+}, Sr^{2+}, Mn^{2+} and H_2O molecules lie inside tubes and channels of the structure. On the basis of microprobe analyses and occupancy refinement of the cation sites, the crystal chemical formula of this charoite can be written as (Z = 1): $(K_{13.88}Sr_{1.0}Ba_{0.32}Mn_{0.36})_{\Sigma 15.56}(Ca_{25.64}Na_{6.36})_{\Sigma 32}[(Si_6O_{11}(O,OH)_6)_2(Si_{12}O_{18}(O,OH)_{12})_2(Si_{17}O_{25}(O,OH)_{18})_2](OH,F)_{4.0}\cdot 3.18H_2O$.

Keywords: charoite, crystal structure analysis, precession electron diffraction (PED), automated electron diffraction tomography (ADT).

Introduction

Charoite, a violet, valuable semi-precious stone is found uniquely in the alkaline intrusion of the Murun massif in Yakutiya, Sakha Republic, Siberia, Russia (Vorob'ev, 2008). The first investigations of this mineral date back more than 50 years. Originally, it was described as the mineral canasite, but more detailed studies revealed that it is a different mineral, and in 1978, it was confirmed as a new mineral species by Rogova *et al*. (1978). However, until recently, its chemical formula, unit-cell parameters, space group and structure have remained unclear.

Charoite occurs in close association with other Ca-bearing alkaline minerals, such as frankamenite ($K_3Na_3Ca_5[Si_{12}O_{30}](OH)F_3\cdot H_2O$), canasite ($K_3Na_3Ca_5[Si_{12}O_{30}](OH,O)_{2.5}F_{1.5}$), miserite

* E-mail: ivrozhdestvenska@mail.ru
DOI: 10.1180/minmag.2010.074.1.159

$(K_3Ca_{10}(Ca,M^{3+})_2[Si_{12}O_{30}][Si_2O_7]_2(O,F,OH)_2\cdot H_2O)$, tokkoite ($K_2Ca_4[Si_7O_{18}(OH)](F,OH)$) and tinaksite ($K_2Ca_2NaTi[Si_7O_{18}(OH)]O$) (Konev *et al*., 1996). The structures of all these minerals are characterized by the occurrence of various types of dreier silicate chains. Close associations, intergrowths and transformation of some minerals into others suggest their structural affinity and metasomatic origin (Rozhdestvenskaya and Nikishova, 2002). Although the structure of charoite was unknown, there was strong evidence that it belongs to the group of alkaline Ca-silicates containing tubular and/or other dreier chains (Frank-Kamenetskaya and Rozhdestvenskaya, 2004).

Despite many attempts to solve the charoite structure, or at least to construct a convincing structural model, the structure and stoichiometry have remained enigmatic, and reported data were partially inconsistent. The crystal chemical formula of charoite, inferred from X-ray powder diffraction, was proposed as $(K,Na)_5(Ca,Ba,Sr)_8[Si_{12}O_{30}][Si_2O_7][Si_4O_9](F,OH)_2\cdot nH_2O$; Z = 4; monoclinic, space group *Pm*, *P*2 or *P*2/*m* with a = 19.6, b = 32.02, c =7.25 Å, β = 94.3º (Nikishova *et al*., 1985).

Chiragov and Shirinova (2004) proposed a model of the charoite structure on the basis of a miserite-like structure in which silicate-oxygen chains are connected to double octahedral bands and form $[Ca_8(Si_{12}O_{30})_2]^{8-}$ structure blocks. These blocks are distributed about y = 0 and ½ and are connected to a $[Si_6O_{16}]^{8-}$ okenite band, or a $[Si_6O_{15}]^{6-}$ okenite net.

Based on the common features of alkaline Ca-silicate structures, X-ray powder diffraction, and on high-resolution transmission electron microscopy (HRTEM), a structural model for charoite was proposed recently by Rozhdestvenskaya *et al*. (2007, 2009*a*). According to this model, charoite is monoclinic (space group $P2_1/m$) with cell parameters a = 32.296, b = 19.651, c = 7.16 Å, β = 96.3º, V = 4517 Å^3, with a general formula $K_{6-7}(Ca,Na)_{18}[(Si_6O_{17})(Si_{12}O_{30})(Si_{18}O_{45})](OH,F)_2\cdot nH_2O$ (Z = 2). The proposed model contained three different one-dimensional infinite silicate radicals: $[Si_6O_{17}]^{10-}$ kinked ribbons, $[Si_{12}O_{30}]^{12-}$ tube radicals, and $[Si_{18}O_{45}]^{18-}$ tube radicals. Following Liebau's (1985) classification terminology for silicates, we will henceforth use the appropriate notation for such silicate radicals: $[Si_6O_{17}]^{10-}$ is a dreier double chain, $[Si_{12}O_{30}]^{12-}$ a tubular loop-branched dreier triple chain and $[Si_{18}O_{45}]^{18-}$ a tubular hybrid dreier quadruple chain. According to the model, the silicate chains are placed between bands formed by edge-sharing $[(Ca,Na)O_6]$ octahedra. The chains and bands extend parallel to the z axis. Potassium ions and H_2O molecules lie at the centres of the tubular chains, and other K ions lie at the centres of eight-membered rings of SiO_4 tetrahedra.

Despite the fact that the model of (Rozhdestvenskaya *et al*., 2007, 2009*a*) displayed important characteristics of the charoite structure, a definitive structure determination was still missing. For such a structure determination the collection of 3D-single crystal diffraction data is essential, but the acquisition of such data is difficult owing to the very small sizes of charoite crystals. Furthermore, our recent studies have shown that the charoite specimens not only contain other silicate minerals and an amorphous phase, but also individual asbestiform microcrystals of charoite having intergrowths of different structural variants, one clearly being monoclinic, a second one being metrically pseudo-orthorhombic, but still monoclinic and a third one with a doubled a parameter (Rozhdestvenskaya *et al*., 2009*b*). Consequently, we decided that for a reliable structure investigation, data from single-phase nanocrystals were required.

Nanoscale electron diffraction provides information from single nanocrystals down to 5 nm in diameter, as the electron beam can be focused down to this size, and the strong scattering of electrons allows a reasonable signal-to-noise ratio even for nanovolumes. Conventional electron diffraction often fails to give enough reflections required for a reliable structure solution. Moreover, it is well known that dynamic effects can result in spurious intensities when they are collected from zones oriented along low-index directions. In order to increase the number of reflections collected from a nanocrystal, and at the same time reduce both the electron dose on the sample and dynamic effects, a newly developed software module called 'automated diffraction tomography' (ADT) (Kolb *et al*., 2007, 2008) was used. The ADT software allows a rich sampling of reciprocal space in order to obtain unambiguous cell parameters even for triclinic crystals, and gives a full 3D-visualization of the reciprocal lattice. As a sample does not need to be oriented along low index zones, dynamic effects are largely reduced. In order to reduce dynamic effects further and to improve intensity integration, ADT can be coupled with 'precession

electron diffraction' (PED) (Vincent and Midgley, 1994; Own, 2005; Avilov *et al*., 2007) whereby almost complete *quasi*-kinematic intensities can be collected by electron diffraction from a nanocrystal. Mugnaioli *et al*. (2009) showed that by this method it is possible to solve small inorganic structures *ab initio* in one step, and also to detect the positions of such elements like oxygen.

In this paper we report our investigations of charoite, performed using a wide range of techniques – HRTEM, selected-area electron diffraction (SAED), microprobe analysis, energy dispersive X-ray spectroscopy (EDX), PED and ADT, which have allowed the structure of charoite to be determined for the first time.

Experimental procedures

Charoite occurs in different morphologies (Evdokimov *et al.*, 1995; Konev *et al.*, 1996). For our study, a charoite sample of light-violet colour was chosen in which individual asbestos-like micro-crystals are elongated along the *z* axis (Fig. 1).

The sample was prepared by crushing in an agate mortar, and also by focused ion beam thinning (FIB). It was studied by conventional and HRTEM and SAED using Philips EM400T, Philips Tecnai F20, Philips Tecnai F30 and JEOL 3010UHR microscopes operated at 100, 200, 300 kV and 300 kV respectively. A Tracor Voyager HP-Ge detector attached to the Tecnai F20 microscope was used for EDX analysis.

The composition of charoite was determined by microprobe analysis using a JEOL JXA8900 electron microprobe using an accelerating voltage of 15 kV and a probe current of 15 nA.

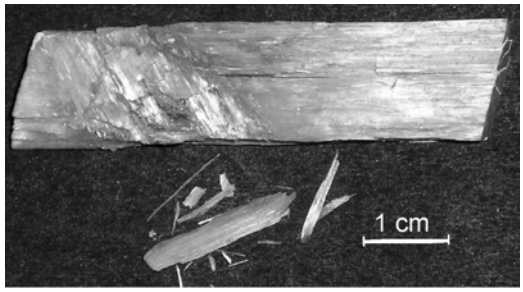

FIG. 1. The morphological variety of the investigated sample of charoite. The crystal length is ~5 cm. The asbestos-like fibres are intimately bound up with each other.

For ADT investigations, the sample was ground, suspended in ethanol and sprayed onto a carbon-coated Cu grid using the sonifier described by Mugnaioli *et al*. (2009). This method made it easy to disperse charoite nanocrystals so that there was no overlap at high tilt angles. The data collection was carried out using a Tecnai F30 S-TWIN transmission electron microscope equipped with a field emission gun and operating at 300 kV. A FISCHIONE tomography holder with a tilt range up to ±70º was used.

The ADT technique allows automatic collection of reflection data sets from a nanocrystal using electron diffraction. The ADT module alternates between scanning transmission electron microscopy (STEM) imaging for crystal tracking in low-dose mode and nanoscale acquisitions (Kolb *et al*., 2007, 2008). The module operates in microprobe STEM mode, and includes routines which allow tracking of a crystal after each tilt step and sequential acquisition of electron diffraction patterns. A 10 μm C2 condenser aperture with a 50 nm beam on the sample was employed in order to produce quasi-parallel illumination of the sample. A mild illumination setting was used, resulting in an electron dose rate of 10−15 e $Å^{-2}$ s^{-1}, suitable also for very beam-sensitive samples. The STEM images were collected by a FISCHIONE high-angular annular dark-field detector (HAADF). The HRTEM images and electron diffraction patterns were taken with a CCD camera (14-bit GATAN 794MSC, 1024×1024 pixels) and acquired by *Digital Micrograph* (GATAN) software. The ADT tilt series were collected in 1º steps with normal parallel illumination and in PED mode (Vincent and Midgley, 1994; Own, 2005; Avilov *et al*., 2007). The PED was performed using the SpinningStar unit developed by NanoMEGAS Company (NanoMEGAS, 2004). The precession angle was 1º and the precession frequency was 100 Hz.

The *ADAP* package (Kolb *et al*., 2007, 2008; Mugnaioli *et al*., 2009) written in *Matlab* was used for data processing, including 3D-reconstruction of diffraction space, automated cell-parameter determination, reflection indexing and intensity integration. For visualization and validation of 3D-data sets, we used the newly developed *ADT-3D* software package written in C++ (Heil *et al*., 2009). The *ab initio* structure solution was performed by direct methods as implemented in

SIR2008, included in the package *IL MILIONE* (Burla *et al*., 2007). The least squares structure refinement was performed using the *SHELXL97* (Sheldrick, 2008) and *CSD* (Akselrud *et al.*, 1989) programs. Electron scattering factors for the refinement were extracted from the *SIR* database.

Results

Bulk sample analysis and charoite polytypism

A TEM investigation of a thin foil of part of the hand specimen containing charoite, previously examined by electron microprobe, shows that it is not homogeneous: crystals of acmite, $NaFeSi_2O_6$, and K-feldspar $K(Fe_{0.1}Al_{0.9}Si_{3.0})O_8$ are also present. The charoite itself has an average chemical composition (11 analyses) of: SiO_2 57.31, TiO_2 0.02, Al_2O_3 0.01, FeO 0.02, MnO 0.35, CaO 21.01, Na_2O 2.29, K_2O 8.35, SrO 1.43, BaO 0.65, F 0.53, subtotalling 91.97 wt.%. The empirical chemical formula calculated on the basis of O = 45 is $(K_{3.28}Sr_{0.26}Ba_{0.08}Mn_{0.09}Fe_{0.01})_{\Sigma 3.72}(Ca_{6.94}Na_{1.37})_{\Sigma 8.31}[Si_{17.65}O_{45}]F_{0.52}$.

In the charoite sample studied here, asbestiform fibres of about 200 nm diameter are almost *z*-parallel, but the *x*–*y* directions are differently oriented (azimuthally disoriented), and they are often separated by amorphous material (Fig. 2*a*,*b*). Analysis, by EDX using TEM, indicates that the amorphous material contains almost no K and less Ca compared with charoite (Fig. 2*c*,*d*).

From [010] SAED patterns on various single fibres, it appears that monoclinic (β = 96º) and metrically orthorhombic (β = 90º) structural

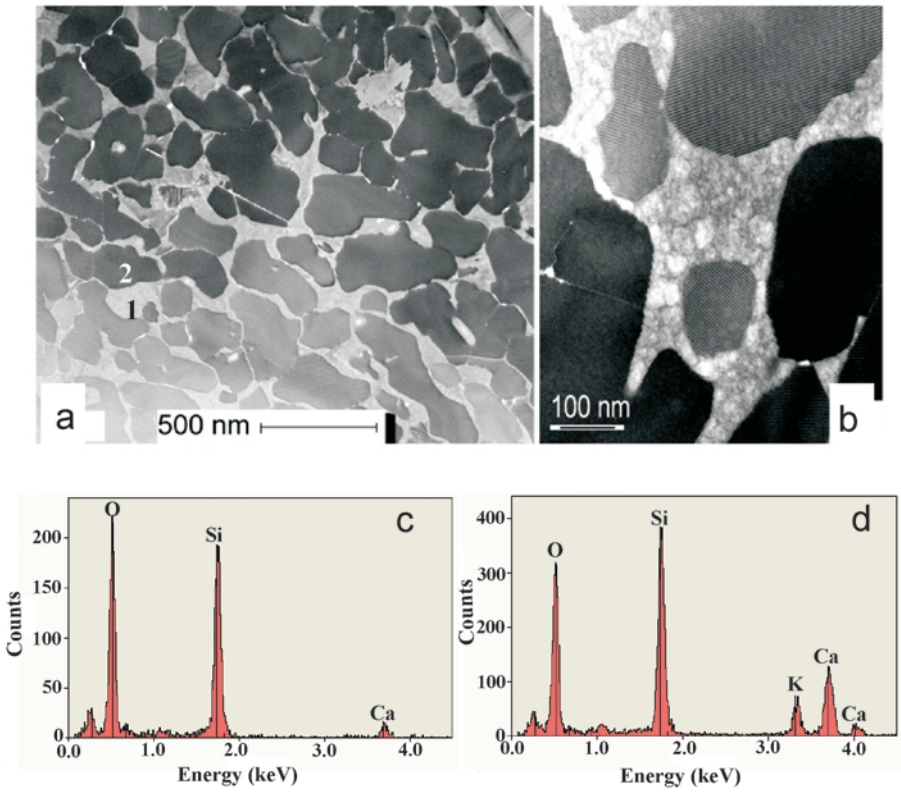

FIG. 2. (*a* and *b*) A [001] TEM image of the charoite sample. (*a*) The FIB lamella is prepared perpendicular to the asbestos-like fibres which have their *z* axis almost parallel but have different (*x, y*) orientations. (*b*) The enlarged image; (100) lattice fringes demonstrate the different fibre orientations. Note the fault with shift of translation in the upper right fibre. The single fibres are separated by 'amorphous material'. (*c*) and (*d*) EDX spectra of charoite. (*c*) Spectrum of area 1, of the 'amorphous material'. (*d*) Spectrum of area 2, of a crystalline fibre. The numbers 1 and 2 in (*a*) indicate typical amorphous and crystalline areas respectively, which were chosen for analyses.

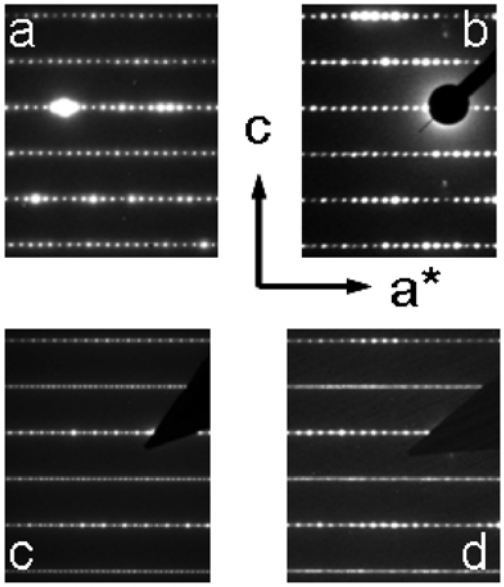

FIG. 3. Slightly tilted [010] SAED patterns of single fibres of various polymorphs of charoite: (*a*) charoite-96, (*b*) charoite-90, (*c*) charoite-2a and (*d*) charoite-d.

variants exist (Fig. 3*a*,*b*). Here, we will distinguish these two polytypes as 'charoite-96' and 'charoite-90' respectively.

Some SAED patterns as well as some HRTEM images (and the corresponding Fourier transforms) show a doubling of the *a* parameter, suggesting a possible third, hitherto unknown, charoite polytype (charoite-2a, Fig. 3*c*; note also the weak reflections in reciprocal rows with $l = 2n$, corresponding to 64 Å). Often, the three structural variants are intimately intergrown as lamellae within the single fibre, having a common axis *a**. Disordered intergrowth of very fine lamellae of the polytypes shows up as diffuse *h*0*l* ($l = 2n+1$) rows ('charoite-d', Fig. 3*d*). Frequently, additional diffraction maxima with uneven distances from the main reflections could be observed in the reciprocal rows *h*0*l* with $l = 2n+1$. Together, with diffuse streaks along *a**, they point at disorder and some kind of (100) micro-lamellae. The micro-lamellae could be caused by stacking faults with fault vector 1/2[001], but micro-twinning of charoite-96 on (100), or intergrowth of charoite-96 and (100) micro-lamellae of charoite-90, also seem to be possible. The [010]-HRTEM images show that the interfaces between lamellar intergrowths can be of various types (Fig. 4). In several [0*kl*] SAED patterns, except [010], additional rows of weak reflections halfway between the rows in *h*0*l* sections were observed, suggesting a doubling of the *c* parameter, which could be associated with ordering along the *z* axis of ions inside the tubular chains.

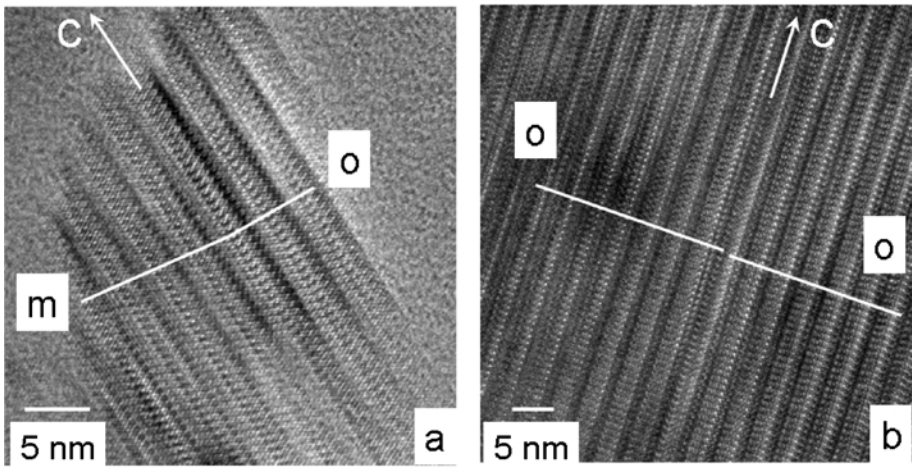

FIG. 4. [010] HRTEM images of intergrowth lamellae (m – monoclinic, charoite-96, o – orthorhombic, charoite-90). In (*a*), the thin crystal has already suffered radiation damage. The thicker crystal in (*b*) shows two orthogonal lamellae separated by a stacking fault with R = 1/2[001].

From a 3D-reconstruction of reciprocal lattices by non-precessed ADT data, the two polytypes, charoite-96 and charoite-90, were easily distinguished. For both polytypes, the only systematic absence is $k = 2n+1$ for $0k0$, arising from a 2_1 screw axis along y. The intensities extracted from the precessed ADT tilt series show unambiguously that charoite-90 is monoclinic. This observation is confirmed by single PED patterns collected along [010] and [110], which show the absence of any mirror elements orthogonal to $h00$ and $00l$ (Fig. 5).

Ab initio structure solution and refinement.

A structurally coherent monophase single fibre of charoite-90 was chosen for intensity collection (Fig. 6*a*). Two tilt series were taken from the same crystal in steps of 1º and in the ranges of 120º and 105º respectively. The tilt axes of the two tilt series were approximately orthogonal. For both series, precessed and non-precessed nanoscale electron diffraction patterns were acquired. The reconstructed 3D-reciprocal space showed a perfectly ordered structure with no disorder streaks (Fig. 6*b*–*d*). Finally, a precessed ADT intensity dataset was obtained by merging the two tilt series. No merging factor was applied. The unit-cell parameters, data acquisition and refinement parameters are given in Table 1. The *hkl* reflection file is available at www.staff.uni-mainz.de/kolb/ADTdata/charoite90.hkl.

The structure solution was performed in space group $P2_1/m$, in accordance with

TABLE 1. Crystallographic data and experimental and refinement parameters for the charoite structure.

a (Å)	31.96(6)
b (Å)	19.64(4)
c (Å)	7.09(1)
β (º)	90.0(1)
V (Å^3)	4450(24)
space group	$P2_1/m$
F_{000}	3396
crystal size (μm^3)	$1 \times 0.2 \times 0.2$
λ (Å)	0.0197
$2\theta_{max}$ (º)	0.96
$(\sin\theta/\lambda)_{max}$	0.424
$(hkl)_{max}$	26, 16, 6
total reflections	8508
resolution (Å)	1.1
$R_{sym.}$ (by *SIR*)	0.133
R_σ	0.0213
Completeness (%)	97
$R_{eqv.}$	0.176
Unique with $\lvert F_o\rvert > 4.0\sigma_F$	2878
R_1	0.17
wR_2*	0.21
GoF	0.97
GoF weighting, w	$1/[\sigma_F^2 + 0.075F_{obs.}^2]$

$R_1 = \Sigma\lvert\lvert F_o\rvert - \lvert F_c\rvert\rvert / \Sigma\lvert F_o\rvert$;
* $wR_2 = \{\Sigma[w(F_o^2 - F_c^2)^2] / \Sigma[w(F_o^2)]\}^{1/2}$;
* $w = 1/[\sigma^2(F_o^2) + (aP)^2 + bP]$, where $P = (F_o^2 + 2F_c^2)/3$;
GoF $= \{\Sigma[w(F_o^2 - F_c^2)]/(n-p)\}^{1/2}$, where n is the number of reflections and p is the number of refined parameters.

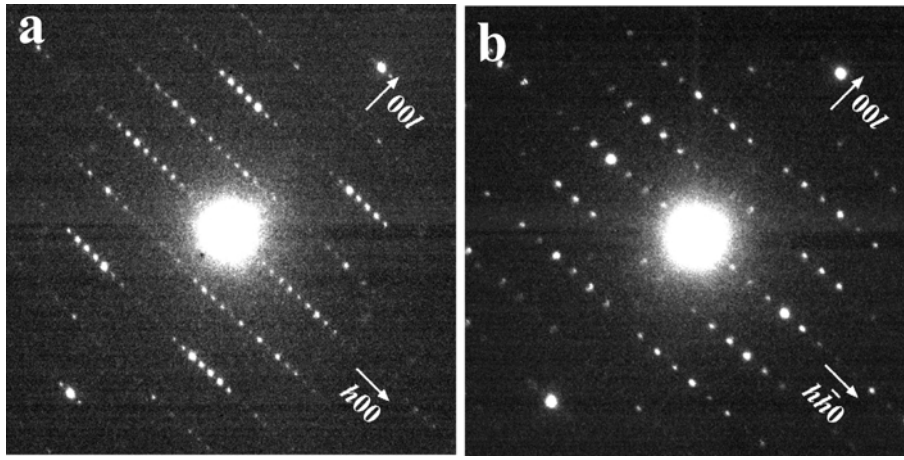

FIG. 5. Main PED zones of charoite-90 showing no mirror symmetry: (*a*) along [010]; (*b*) along [110].

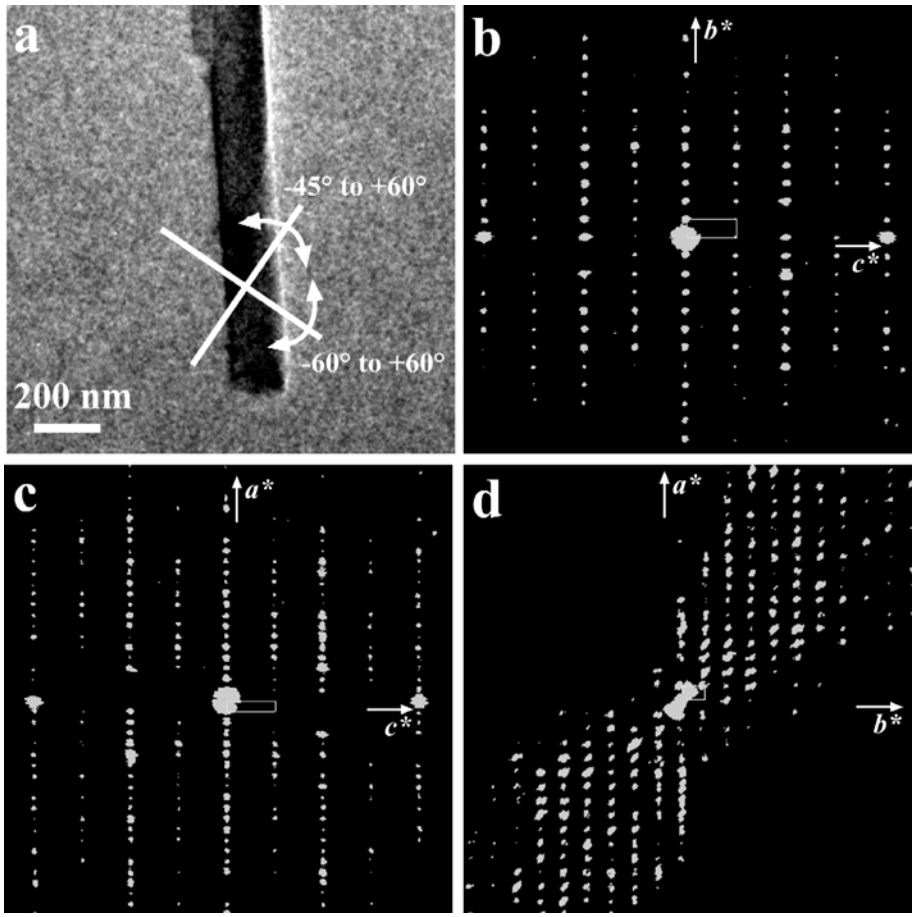

FIG. 6. (*a*) Crystal selected for the precessed ADT data acquisitions. The tilt axes for the two acquisitions are sketched in white. Reconstructed 3D-reciprocal space for charoite-90 polytype. (*b*) [100] view, (*c*) [010] view, (*d*) [001] view.

Rozhdestvenskaya *et al.* (2007, 2009*a*). The structure was solved *ab initio* by direct methods using *SIR2008* (Burla *et al*., 2007) using a fully kinematic approach, i.e. intensities were assumed to be proportional to F^2_{hkl}. The best solution has R = 0.231 and an overall atom displacement parameter U_{overall} of 0.039 Å^2. The best solution is much better, both in terms of R value and figure of merit, than the cloud of incorrect solutions (Fig. 7). A total of 8 Ca, 20 Si and 47 O positions were correctly identified. The missing 4 Os of the framework and the channel content (3 H_2O molecules, 7 K and 1 Sr positions) were detected in the first difference-Fourier map calculated by *SHELXL97* (Sheldrick, 1997).

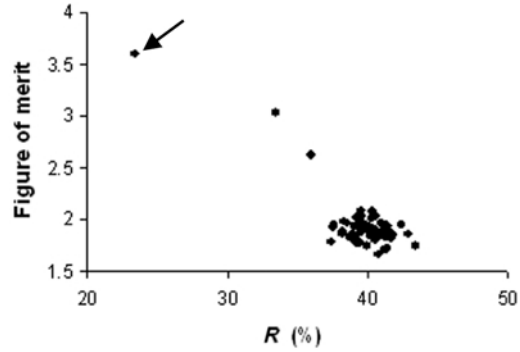

FIG. 7. Cloud of solutions by *SIR2008*: the correct solution is far from the cloud of wrong solutions. The arrow marks the correct solution.

The least squares refinements using *SHELXL97* (Sheldrick, 1997) and *CSD* (Akselrud *et al.*, 1989), with 2878 reflections, $F_{hkl} > 4\sigma_F$, converged to unweighted/weighted residuals $R_1/wR_2 = 0.173/0.21$. The number of independent atom positions is 90, the number of free variables 707. Provisional refinement of site occupancies was also performed. The refinement was not perfect because the intensities of equivalent reflections varied too much ($R_{eqv.} = 0.176$), and no geometrical restraints or constraints were applied. Nevertheless, the data were sufficiently precise to reveal the relevant topological and geometrical features of the structure, and to find sites with mixed occupancy of cations. The refined atom positions, isotropic displacement parameters and site occupancies are given in Table 2, and selected bond lengths are shown in Table 3.

TABLE 2. Atom coordinates, isotropic and equivalent isotropic displacement parameters (Å^2) and position occupancies of charoite structure.

Site	N*	*x*	*y*	*z*	U_{iso}/U_{eq}† × 100	Occupancy‡
Na(1)	4	0.9654(3)	0.0640(5)	0.6206(12)	5.8(4)	0.64(3) Na +0.36 Ca
Na(2)	4	0.9668(4)	0.0759(7)	0.1341(15)	6.0(5)	0.95(3) Na +0.05Ca
Ca(1)	4	0.8769(2)	0.1474(3)	0.3786(9)	5.8(3)	
Ca(2)	4	0.8780(2)	0.1446(3)	0.8814(9)	5.7(2)	
Ca(3)	4	0.5412(2)	0.0429(3)	0.8787(8)	5.2(2)	
Ca(4)	4	0.5415(2)	0.0397(3)	0.3768(8)	4.5(2)	
Ca(5)	4	0.3478(2)	0.0715(3)	0.1215(8)	5.3(2)	
Ca(6)	4	0.3484(2)	0.0706(4)	0.6257(8)	5.7(3)	
K(1)	2	0.4857(3)	¼	0.1277(13)	5.1(2)	
K(2)	2	0.5984(3)	¼	0.6310(12)	5.1(2)	
K(3)	4	0.7397(2)	0.1140(4)	0.6273(11)	7.4(2)	
K(4)	2	0.3562(3)	¼	0.8515(14)	8.8(3)	0.57 K + 0.18 Mn + 0.16 Ba
K(5)	2	0.6903(7)	¼	0.135(3)	9.6(7)	0.55(2) K
K(6)	4	0.2060(3)	0.0453(4)	0.8787(11)	5.4(2)	0.79(1) K
K(7)	4	0.0495(12)	0.196(2)	0.870(5)	1.6(11)	0.12(1) K
Sr	2	0.3419(5)	¼	0.380(2)	7.8(6)	0.50(2) Sr
Si(1)	4	0.4975(3)	0.1754(5)	0.6261(15)	6.8(4)	
Si(2)	4	0.4425(3)	0.1033(5)	0.3372(11)	4.8(3)	
Si(3)	4	0.4418(3)	0.1051(5)	0.9050(12)	5.7(4)	
Si(4)	4	0.5881(3)	0.1723(4)	0.1272(12)	5.5(3)	
Si(5)	4	0.6399(3)	0.1039(4)	0.4197(12)	4.4(3)	
Si(6)	4	0.6381(3)	0.1014(5)	0.8464(15)	6.9(4)	
Si(7)	4	0.7036(3)	0.0558(4)	0.1332(11)	5.1(3)	
Si(8)	4	0.7858(2)	0.1385(5)	0.1249(11)	4.4(3)	
Si(9)	2	0.7921(5)	¼	0.838(2)	8.3(6)	
Si(10)	2	0.7918(4)	¼	0.416(2)	5.3(5)	
Si(11)	4	0.2660(3)	0.1753(6)	0.6606(14)	6.8(4)	
Si(12)	4	0.2662(3)	0.1792(5)	0.0792(11)	5.6(4)	
Si(13)	4	0.2518(3)	0.0672(5)	0.3719(13)	6.3(4)	
Si(14)	4	0.8288(3)	0.0161(4)	0.6262(12)	5.2(3)	
Si(15)	4	0.1059(2)	0.0259(4)	0.0964(12)	4.0(3)	
Si(16)	4	0.1072(3)	0.0236(5)	0.6504(13)	6.2(4)	
Si(17)	4	0.0573(3)	0.1071(5)	0.3699(13)	6.3(4)	
Si(18)	2	0.0202(3)	¼	0.3784(13)	2.1(4)	
Si(19)	2	0.9469(3)	¼	0.0906(14)	10.5(9)	
Si(20)	2	0.9479(3)	¼	0.6600(15)	8.0(7)	
O(1)	2	0.5136(6)	¼	0.632(3)	6.5(8)	
O(2)	4	0.4665(4)	0.1712(8)	0.800(2)	7.1(6)	
O(3)	4	0.4642(5)	0.1637(8)	0.452(2)	7.4(6)	
O(4)	4	0.5340(4	0.1251(8)	0.620(2)	7.2(6)	
O(5)	4	0.4467(6)	0.1271(10)	0.114(3)	11.6(9)	

TABLE 2 (*contd.*)

Site	N*	*x*	*y*	*z*	U_{iso}/U_{eq}† × 100	Occupancy‡
O(6)	4	0.3943(5)	0.1112(8)	0.392(2)	7.3(6)	
O(7)	4	0.4672(5)	0.0316(7)	0.386(2)	7.6(6)	
O(8)	4	0.3915(5)	0.1087(7)	0.866(2)	6.2(5)	
O(9)	4	0.4664(5)	0.0352(7)	0.869(2)	6.0(5)	
O(10)	2	0.5717(7)	¼	0.112(3)	7.5(9)	
O(11)	4	0.6170(4)	0.1664(6)	0.311(2)	4.5(5)	
O(12)	4	0.6164(4)	0.1687(9)	0.956(2)	7.2(6)	
O(13)	4	0.5504(5)	0.1215(8)	0.138(2)	7.2(6)	
O(14)	4	0.6871(4)	0.1021(7)	0.310(2)	5.2(5)	
O(15)	4	0.6516(7)	0.1308(8)	0.633(3)	9.9(8)	
O(16)	4	0.6146(5)	0.0357(8)	0.417(2)	7.9(6)	
O(17)	4	0.6839(5)	0.0952(8)	0.955(2)	8.1(6)	
O(18)	4	0.6132(4)	0.0321(7)	0.862(2)	7.2(6)	
O(19)	4	0.7539(4)	0.0732(7)	0.129(2)	5.7(5)	
O(20)	4	0.3087(5)	0.0188(10)	0.872(2)	8.6(7)	
O(21)	4	0.7683(4)	0.1888(8)	0.317(2)	6.2(5)	
O(22)	4	0.7725(5)	0.1845(9)	0.949(2)	8.1(6)	
O(23)	4	0.8326(5)	0.1144(9)	0.132(2)	7.7(6)	
O(24)	2	0.7794(6)	¼	0.629(2)	4.4(7)	
O(25)	2	0.8433(6)	¼	0.866(3)	5.6(7)	
O(26)	2	0.8407(6)	¼	0.390(2)	4.7(7)	
O(27)	2	0.2489(7)	¼	0.590(3)	8.9(11)	
O(28)	4	0.2418(4)	0.1164(6)	0.549(2)	5.4(5)	
O(29)	4	0.2493(5)	0.1674(8)	0.869(2)	7.5(6)	
O(30)	4	0.3163(5)	0.1777(8)	0.627(2)	7.4(6)	
O(31)	2	0.2452(6)	¼	0.167(2)	5.4(8)	
O(32)	4	0.2409(4)	0.1193(8)	0.183(3)	8.0(6)	
O(33)	4	0.3180(5)	0.1759(9)	0.101(2)	7.6(6)	
O(34)	4	0.2218(3)	0.0062(6)	0.360(2)	3.7(4)	
O(35)	4	0.2977(6)	0.0451(9)	0.388(3)	10.2(8)	
O(36)	4	0.1529(5)	0.0162(7)	0.186(3)	8.3(6)	
O(37)	4	0.1517(5)	0.0180(8)	0.548(2)	7.5(6)	
O(38)	4	0.8352(5)	0.0925(10)	0.638(2)	8.4(7)	
O(39)	4	0.0835(5)	0.0881(8)	0.193(2)	7.7(6)	
O(40)	4	0.1135(4)	0.0468(7)	0.8681(15)	4.9(5)	
O(41)	4	0.9212(4)	0.0443(8)	0.890(2)	6.2(5)	
O(42)	4	0.9191(5)	0.0434(9)	0.365(2)	6.9(6)	
O(43)	4	0.0853(6)	0.0872(9)	0.556(2)	8.4(7)	
O(44)	4	0.0510(5)	0.1842(10)	0.366(2)	8.6(7)	
O(45)	4	0.0157(5)	0.0603(7)	0.371(2)	6.6(5)	
O(46)	2	0.9919(10)	¼	0.185(3)	10.6(12)	
O(47)	2	0.9941(8)	¼	0.567(5)	13.5(16)	
O(48)	2	0.9655(5)	¼	0.879(3)	4.8(7)	
O(49)	4	0.9256(4)	0.1811(8)	0.131(2)	7.0(6)	
O(50)	4	0.9249(4)	0.1809(7)	0.620(2)	5.8(5)	
OH	4	0.0200(8)	0.054(2)	0.901(4)	15.4(13)	0.5 OH + 0.5 F
$H_2O(1)$	2	0.7140(13)	¼	0.602(6)	1.3(11)	0.31(3) O
$H_2O(2)$	4	0.1754(8)	0.2115(14)	0.339(3)	4.3(6)	0.46(3) O
$H_2O(3)$	2	0.400(2)	¼	0.547(8)	6.0(15)	0.36(4) O

* N − multiplicity,† $U_{eq} = 1/3[U_{11}\, a^{*2}\, a^2 + ... + 2U_{23}\, b^*\, c^*\, b\, c \cos(\alpha)]$, ‡ occupancy of mixed sites only is shown. All other sites are fully occupied by the element.
Only K(1−7) and the oxygens of H_2O(1−3) were refined isotropically (U_{iso}); all other sites were refined anisotropically.

Tables of anisotropic displacement parameters and structure factors have been deposited with the Principal Editor of *Mineralogical Magazine* and are available from www.minersoc.org/pages/e_journals/dep_mat_mm.html.

The structure of charoite can be visualized as being composed of three different silicate chains: a dreier double chain, $[Si_6O_{17}]^{10-}$, a tubular loop-branched dreier triple chain, $[Si_{12}O_{30}]^{12-}$ and a tubular hybrid dreier quadruple chain,

TABLE 3. Bond lengths (Å) in the charoite structure.

Na(1)–O(42)	2.37(4)	Na(2)–O(45)	2.32(5)	Ca(1)–O(26)	2.32(5)	Ca(2)–O(25)	2.35(5)
–O(45)	2.39(4)	–O(42)	2.32(5)	–O(23)	2.34(4)	–O(23)	2.37(4)
–O(41)	2.41(4)	–O(41)	2.34(4)	–O(50)	2.39(4)	–O(41)	2.41(5)
–O(45)	2.51(5)	–OH	2.41(5)	–O(49)	2.44(4)	–O(38)	2.43(4)
–O(50)	2.64(5)	–O(49)	2.45(5)	–O(42)	2.45(5)	–O(49)	2.44(4)
–OH	2.65(5)	–OH	2.61(5)	–O(38)	2.51(4)	–O(50)	2.49(4)
Average	2.49		2.41		2.41		2.41
Ca(3)–O(18)	2.31(6)	Ca(4)–O(7)	2.20(3)	Ca(5)–O(33)	2.27(5)	Ca(6)–O(8)	2.32(4)
–O(9)	2.37(3)	–O(9)	2.30(3)	–O(18)	2.39(5)	–O(30)	2.34(5)
–O(7)	2.40(3)	–O(16)	2.35(6)	–O(8)	2.40(4)	–O(6)	2.35(4)
–O(9)	2.40(6)	–O(13)	2.35(3)	–O(20)	2.40(4)	–O(20)	2.39(4)
–O(13)	2.42(3)	–O(7)	2.38(6)	–O(35)	2.53(5)	–O(35)	2.39(5)
–O(4)	2.45(3)	–O(4)	2.42(3)	–O(6)	2.55(4)	–O(16)	2.42(5)
Average	2.39		2.33		2.42		2.37
Si(1)–O(4)	1.53(6)	Si(2)–O(6)	1.60(6)	Si(3)–O(5)	1.55(3)	Si(4)–O(12)	1.51(4)
–O(1)	1.55(4)	–O(3)	1.60(4)	–O(9)	1.60(5)	–O(13)	1.57(6)
–O(2)	1.59(4)	–O(7)	1.65(5)	–O(8)	1.63(6)	–O(11)	1.60(4)
–O(3)	1.65(4)	–O(5)	1.66(3)	–O(2)	1.69(5)	–O(10)	1.62(4)
Average	1.58		1.63		1.62		1.57
Si(5)–O(16)	1.56(5)	Si(6)–O(18)	1.58(5)	Si(7)–O(20)	1.52(5)	Si(8)–O(23)	1.57(6)
–O(11)	1.62(4)	–O(17)	1.66(6)	–O(17)	1.61(4)	–O(22)	1.59(3)
–O(15)	1.65(3)	–O(12)	1.68(5)	–O(19)	1.64(5)	–O(19)	1.64(3)
–O(14)	1.70(6)	–O(15)	1.68(3)	–O(14)	1.64(5)	–O(21)	1.77(3)
Average	1.63		1.65		1.60		1.64
Si(9)–O(24)	1.54(3)	Si(10)–O(24)	1.56(3)	Si(11)–O(29)	1.58(3)	Si(12)–O(29)	1.60(3)
–O(22) × 2	1.64(4)	–O(26)	1.57(6)	–O(28)	1.60(4)	–O(32)	1.61(5)
–O(25)	1.65(7)	–O(21) × 2	1.58(5)	–O(30)	1.63(6)	–O(31)	1.66(4)
				–O(27)	1.64(4)	–O(33)	1.66(6)
Average	1.62		1.57		1.61		1.63
Si(13)–O(35)	1.53(6)	Si(14)–O(38)	1.52(5)	Si(15)–O(39)	1.58(5)	Si(16)–O(42)	1.56(5)
–O(34)	1.54(5)	–O(37)	1.54(4)	–O(41)	1.63(5)	–O(43)	1.58(5)
–O(28)	1.62(3)	–O(36)	1.59(4)	–O(36)	1.64(6)	–O(37)	1.60(6)
–O(32)	1.72(3)	–O(34)	1.68(6)	–O(40)	1.69(2)	–O(40)	1.62(2)
Average	1.60		1.58		1.64		1.59
Si(17)–O(44)	1.53(5)	Si(18)–O(47)	1.58(5)	Si(19)–O(46)	1.59(6)	Si(20)–O(48)	1.65(3)
–O(39)	1.55(4)	–O(44) × 2	1.63(5)	–O(49) × 2	1.54(5)	–O(50) × 2	1.57(5)
–O(45)	1.62(6)	–O(46)	1.64(5)	–O(48)	1.61(3)	–O(47)	1.62(6)
–O(43)	1.64(4)						
Average	1.59		1.62		1.57		1.60
Sr–H_2O(3)	2.20(8)	K(1)–O(5) × 2	2.72(5)	K(2)–O(1)	2.71(6)	K(4)–O(30) × 2	2.48(4)
–O(30) × 2	2.40(4)	–O(10)	2.75(6)	–O(12) × 2	2.86(3)	–H_2O(3)	2.57(7)
–O(33) × 2	2.57(4)	–O(2) × 2	2.86(3)	–O(11) × 2	2.86(5)	–O(33) × 2	2.60(4)
–O(6) × 2	3.20(5)	–O(3) × 2	2.94(3)	–O(15) × 2	2.89(5)	–O(22)	2.87(4)
–O(13) × 2	3.26(5)	–O(4) × 2	3.20(5)	–O(8) × 2	3.00(5)		
Average	2.65		2.92		2.93		2.68

$[Si_{17}O_{43}]^{18-}$ (Fig. 8*a*). All chains run parallel the *z* axis. The chains are bonded by their apical O atoms to (Ca,Na)-octahedra bands of various widths, which are also parallel *z* (Fig. 8*b*). K^+, Ba^{2+}, Sr^{2+}, Mn^{2+} and H_2O molecules are located inside the silicate chains.

Columns of octahedra

In the structure of charoite, columns of edge-sharing alternating Na(1)-Na(2), Ca(1)-Ca(2), Ca(3)-Ca(4), Ca(5)-Ca(6) octahedra extend parallel to the *z* axis (Fig. 8*b*). The columns of Na(1)-Na(2), as well as of Ca(3)-Ca(4) octahedra across the centre of symmetry form a ribbon two octahedra wide. The columns of Ca(1)-Ca(2) octahedra are joined by shared edges with the columns of Na(1)-Na(2) octahedra and build a block four octahedra wide (Fig. 8*a*). The apical O atoms O(25) and O(26) link two such blocks to form a continuous zigzag sheet parallel to (100). The columns of Ca(5)-Ca(6) octahedra are linked with the columns of Ca(3)-Ca(4) octahedra *via* common apical O atoms O(16) and O(18). These octahedra form isolated blocks.

Calcium/sodium isomorphism is typical for Ca-bearing alkaline silicates (Rozhdestvenskaya and Nikishova, 2002). However, the octahedrally-coordinated sites in charoite are predominantly occupied by Ca. It is, therefore, surprising that in charoite only two octahedra, Na(1) and Na(2), have mixed Ca/Na occupancy (Table 2). The mean bond distance *M*−O of octahedra is 2.40 Å and varies from 2.33 to 2.49 Å (Table 3).

Silicate chains

The dreier double chain, $[Si_6O_{17}]^{10-}$, is of the same type as the chain found in the xonotlite structure (Fig. 9*a*,*d*). The tubular dreier triple chain, $[Si_{12}O_{30}]^{12-}$ (Fig. 9*b*,*e*), differs from the chains of identical stoichiometry found in the structures of frankamenite and miserite. In charoite, this tubular chain is formed by three loop-branched dreier single chains and has threefold symmetry. Such loop-branched dreier single chains are known from the structure of synthetic $Li_2Mg_2[Si_4O_{11}]$ (Czank and Bissert, 1993).

The tubular hybrid dreier quadruple chain, $[Si_{17}O_{43}]^{18-}$ (Fig. 9*c*,*f*,*h*), differs from the tubular dreier chain, $[Si_{18}O_{45}]^{18-}$, which was proposed earlier (Rozhdestvenskaya *et al*., 2007, 2009*a*), and has a more complex structure. It consists of two loop-branched dreier single chains (tetrahedra 14, 15, 16, 17), a dreier single chain (tetrahedra 18, 19, 20) and a dreier double chain (tetrahedra 11, 12, 13 and 11m, 12m, 13m).

The dreier single chain is similar to that found in pectolite and the dreier double chain is of the type found in okenite. It is of interest that tetrahedron T(18) of this large tubular chain is connected to four other tetrahedra, thus its connectivity is more typical for tetrahedra in framework structures than for tetrahedra in chain silicates.

The three different chains of the structure lie on the mirror plane and alternate along the *x* axis (Fig. 10). The smaller tubular chain is surrounded

Table 3 (*contd*.).

K(3)−O(34)	2.66(5)	K(5)−O(21) × 2	3.05(6)	K(6)−O(19)	2.66(5)	K(7)−O(48)	2.89(7)
−H_2O(1)	2.80(5)	−O(11) × 2	3.12(6)	−O(29)	2.77(5)	−OH	2.94(7)
−O(21)	2.80(3)	−O(12) × 2	3.12(6)	−O(36)	2.82(4)	−O(47)	2.98(6)
−O(14)	2.82(4)	−O(14) × 2	3.16(4)	−O(32)	2.83(4)	−O(46)	3.09(6)
−O(15)	2.83(6)	−O(22) × 2	3.21(6)	−O(28)	2.95(4)	−O(43)	3.29(5)
−O(22)	2.87(4)	−O(17) × 2	3.31(4)	−O(37)	2.96(4)	−O(39)	3.30(5)
−O(17)	2.95(4)	−H_2O(1)	3.39(6)	−O(40)	2.96(6)	Average	3.08
−O(24)	2.96(5)	Average	3.18	−O(20)	3.32(6)		
−O(38)	3.08(6)			−O(23)	3.37(6)	−K(7)	2.13(6)
Average	2.96				2.96		
H_2O(1)−O(24)	2.10(8)	H_2O(2)−O(31)	2.65(6	H_2O(3)−Sr	2.20(8)		
−K(3) × 2	2.80(5)	−O(32)	2.98(6)	−K(4)	2.57(7)		
−O(21) × 2	2.92(6)	−O(27)	3.04(6)	−O(3) × 2	2.75(7)		
−O(15) × 2	3.08(6)	−O(28)	3.19(6)	−O(6) × 2	2.94(5)		
−K(5)	3.39(8)	Average	2.97	−O(30) × 2	3.07(8)		
Average	2.81			−O(2) × 2	3.19(7)		
		−H_2O(2)	1.51(4)	Average	2.87		

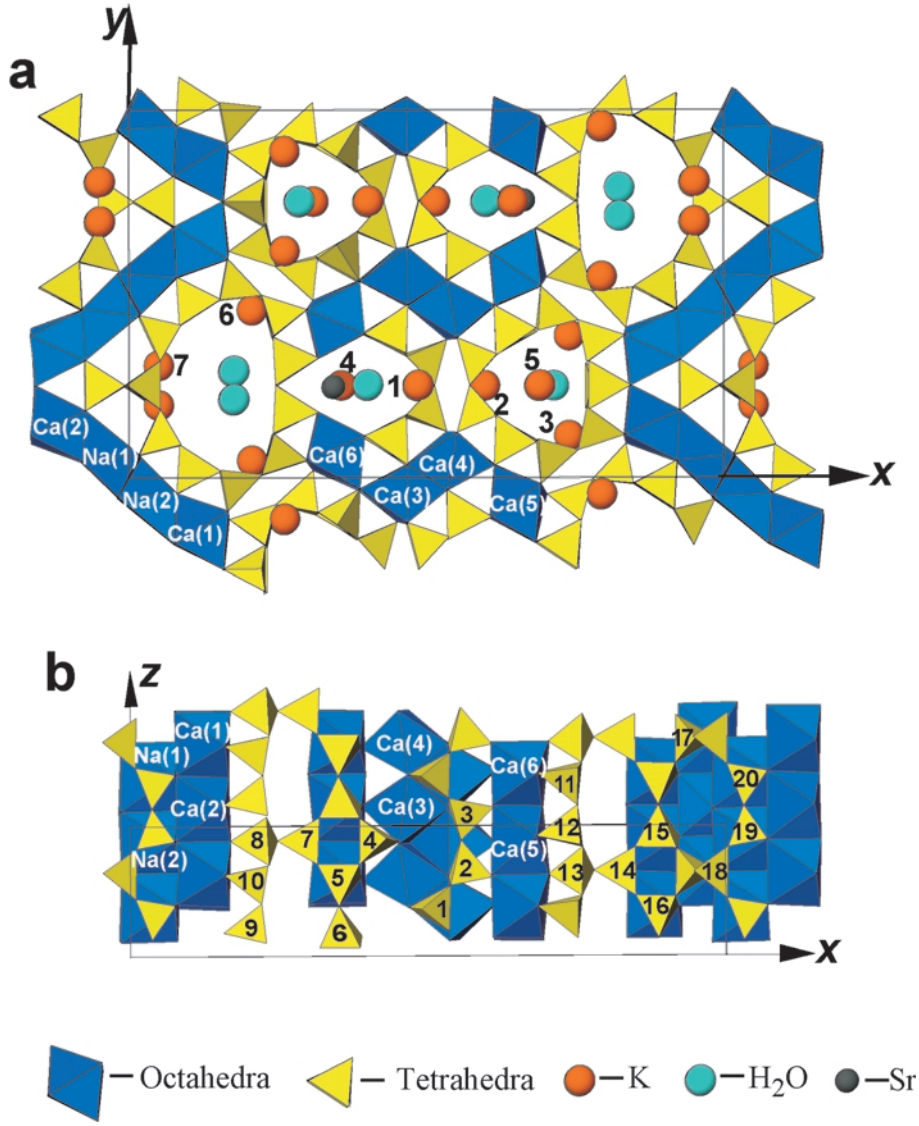

FIG. 8. The crystal structure of charoite-90. (*a*) In projection on plane (001) and (*b*) part of structure $-0.25 < y < 0.25$ in projection on plane (010). For simplicity, only the front side of the silicate chains is shown. The numbers on Figs 8 and 9 correspond to the atomic sites in Table 2.

by one double chain and two of the larger tubular chains in such a way that each one of the three horizontal $[Si_2O_7]^{6-}$ groups of the smaller tubular chain has, as neighbour, a horizontal $[Si_2O_7]^{6-}$ group of one of the surrounding chains (Fig. 10).

The double chain $[Si_6O_{17}]^{10-}$ joins with blocks of octahedra Ca(3)-Ca(4) – Ca(5)-Ca(6) (Fig. 8*a*, 11*a*). The tetrahedra Si(8), Si(9) and Si(10) of the smaller tubular chain $[Si_{12}O_{30}]^{12-}$ are joined with two columns of Ca(1)-Ca(2) octahedra and the tetrahedra Si(4)-Si(7) join to columns of octahedra Ca(3)-Ca(4) and Ca(5)-Ca(6) (Fig. 8*a*, 11*b*). Tetrahedra Si(11), Si(12) and Si(13) of the larger tubular chain $[Si_{17}O_{43}]^{18-}$ are connected to columns of Ca(5)-Ca(6) octahedra (Fig. 8*a*, 11*c*), and, finally, Si(15), Si(16), Si(17), Si(19) and

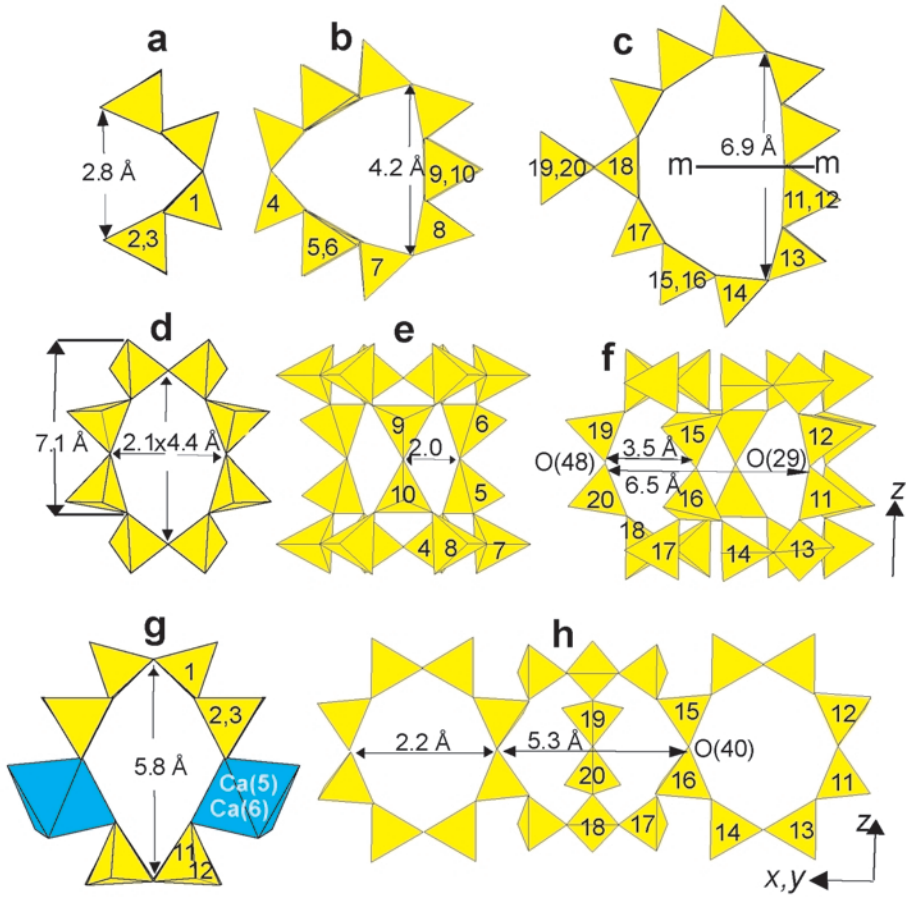

FIG. 9. Structure of silicate chains in charoite-90. (*a*,*d*) Bent dreier double chain $[Si_6O_{17}]^{10-}$. (*b*,*e*) Tubular loop-branched dreier triple chain $[Si_{12}O_{30}]^{12-}$. (*c*,*f*,*h*) Tubular hybrid dreier quadruple chain $[Si_{17}O_{43}]^{18-}$. (*a*,*b*,*c*) [001] projections. (*d*,*e*,*f*) [100] projections. (*f*) The chain is slightly tilted from [100] for better visualization. (*h*) The same chain cut along the mirror plane *m* and unfolded onto (100). (*g*) The tube formed by the dreier double chain, $[Si_6O_{17}]^{10-}$, the Ca(5) and Ca(6) octahedra and the Si(11) and Si(12) tetrahedra shown in [001] projection.

Si(20) tetrahedra join with blocks of Na(1)-Na(2) – Ca(1)-Ca(2) octahedra (Fig. 8*a*, 11*d*). Tetrahedron Si(18) is unique in that it connects to four other tetrahedra of the same chain (Fig. 8*a*, 9*h*, 11*d*).

Horizontal $[Si_2O_7]^{6-}$ groups of each chain connect the separate bands of Ca-octahedra in such a way that apical O atoms of neighbouring $[Si_2O_7]^{6-}$ groups are joined to different apices of vertical edges of octahedra and, therefore, adjacent chains are shifted relative to each other by half a translation along the *z* axis (Fig. 8*a*).

The mean bond lengths in the tetrahedra range between 1.57 and 1.65 Å (Table 3). The mean O–Si–O angles are in the range 109.1–109.4°. However, we point out that the shortest and longest bond lengths found (1.51 and 1.77 Å respectively) are probably not realistic. This large deviation from standard values is almost certainly due to the fact that the refinement is not perfect, at least when considered from the point of view of standard X-ray diffraction methods applied to standard crystals with small structures. This imperfection is also reflected in the correspondingly large e.s.d. of lattice parameters, bond lengths and angles.

Tetrahedra Si(9), Si(10), Si(18), Si(19) and Si(20) lie in the mirror plane. The tubular chains

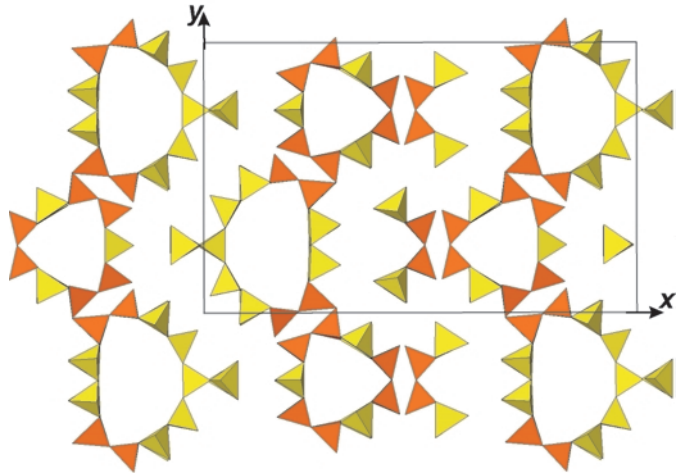

FIG. 10. The arrangement of the three silicate chains in projection on plane (001). Horizontal groups $[Si_2O_7]^{6-}$ are red.

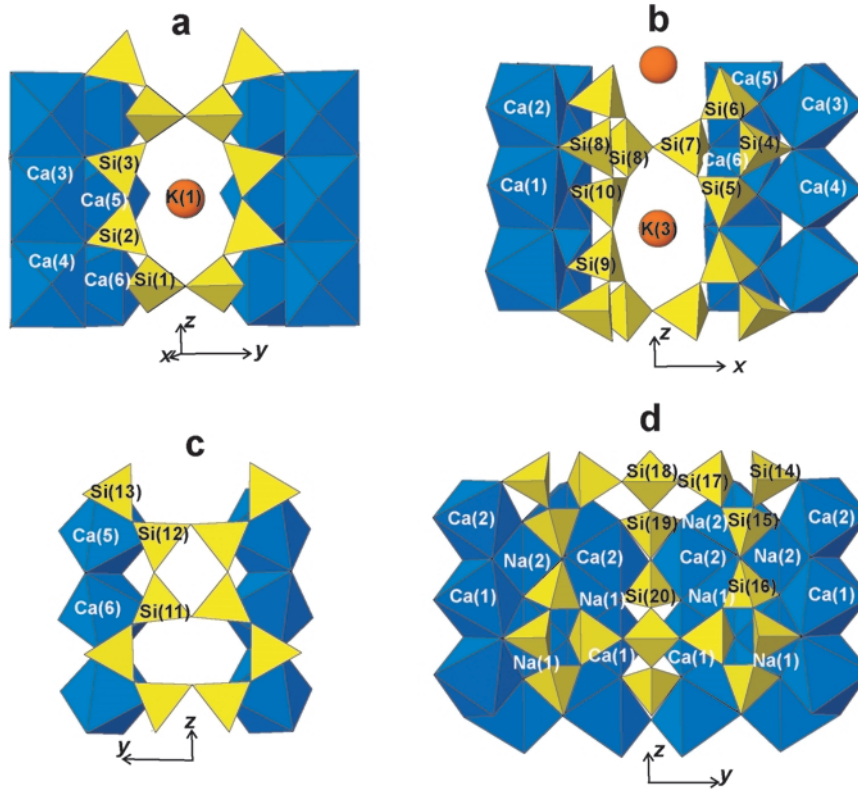

FIG. 11. The connection of silicate chains with octahedra bands (along *z* axis). (*a*) A bent dreier double chain $[Si_6O_{17}]^{10-}$ between two Ca(3)-Ca(4) – Ca(5)-Ca(6) octahedra bands. (*b*) A part of the tubular chain $[Si_{12}O_{30}]^{12-}$ between Ca(1)-Ca(2) columns and a Ca(3)-Ca(4) – Ca(5)-Ca(6) band. (*c*) A part of the tubular chain $[Si_{17}O_{43}]^{18-}$ connecting two Ca(5)-Ca(6) octahedral columns. (*d*) A part of the tubular chain $[Si_{17}O_{43}]^{18-}$ between two Na(1)-Na(2) – Ca(1)-Ca(2) bands.

exhibit free channels along the chains, which are defined by nine- and eleven-membered rings of tetrahedra, '9MR' and '11MR' respectively (Fig. 9*b*,*c*). The double chain $[Si_6O_{17}]^{10-}$ forms a tube together with Ca(5) and Ca(6) octahedra and Si(11) and Si(12) tetrahedra (Fig. 9*g*). The tubes extend along the *z* axis. All chains also have windows of eight-membered rings '8MR' of various free diameters. The free diameter of the channels and windows has been estimated from the distance between O atoms across the ring minus 2.7 Å (assuming the ionic radius of O to be 1.35 Å). The sizes of the free diameters are shown in Fig. 9*a*–*h*. The channel of the large tubular chain $[Si_{17}O_{43}]^{18-}$ has a structural protrusion formed by two Si(15) and Si(16), four Si(17), two Si(18), Si(19) and Si(20) tetrahedra. Thereby, a big cavity is formed in which the largest free diameters are 5.3 Å [O(40)–O(40)] and 6.5 Å [O(48)–O(29)] (Fig. 9*f*,*h*). This cavity is delimited by two symmetrically equivalent '8MR's with free diameters 2.2×4.4 Å and two more, again symmetrically equivalent, '8MR's with free diameters 3.5×4.4 Å.

Sites of K^+, Sr^{2+}, Mn^{2+}, Ba^{2+} and H_2O molecules

In the '8MR' windows on the side of the basal Os of all silicate chains, the K atoms are located in the sites K(1), K(2), K(3), K(6) (c.f. Fig. 8*a*, 11*a*,*b*), and have nine-fold coordination. The mean bond length K–O is 2.94 Å (Table 3). Six Os of the '8MR' within which the K atoms are located and three Os of the adjacent chain take part in the charge compensation for each of these cations, thus providing an additional link between adjacent chains.

Another K atom, K(5), is located on the axis of the tubular chain $[Si_{12}O_{30}]^{12-}$ (Fig. 8*a*). It has weaker bonds (mean bond length K–O = 3.18 Å) in the structure, this site is not fully occupied (occ. = 0.55 K). The $H_2O(1)$ molecule can be located at 1/2 of the translation along the *z* axes from that K site in the tube cavity. This site is also not fully occupied (occ. = 0.31 O). The O of the H_2O group is linked with K in site K(3), located in the '8MR' window; bond length K(3)–$H_2O(1)$ = 2.80 Å.

The cavity within the large tubular chain $[Si_{17}O_{43}]^{18-}$ is nearly empty. Only two small peaks were found in a difference-Fourier map. Taking into account the distances from these peaks to the nearest O atoms, we infer that K atoms are located in site K(7) (mean bond length K(7)–O = 3.08 Å) and H_2O molecules in site $H_2O(2)$ (mean bond length $H_2O(2)$–O = 2.97 Å) (Table 3). The refined occupancies for K(7) are 0.12 K and 0.46 O for $H_2O(2)$ (Table 2). The short distances K(7)–K(7) = 2.13 and $H_2O(2)$–$H_2O(2)$ = 1.51 Å should be considered admissible since the sites are only partly occupied.

The interior of the tube formed by the bent ribbon $[Si_6O_{17}]^{10-}$, the Ca(5), Ca(6) octahedra and the Si(11), Si(12) tetrahedra, has a higher occupancy than the $[Si_{17}O_{43}]^{18-}$ tubular chain (Fig. 8*a*). Three peaks were found on Fourier maps. From the distances of these peaks from nearest O atoms, we infer that Sr^{2+} is the occupant (mean bond length Sr–O = 2.65 Å). The refinement showed that the occupancy of the Sr site is 0.50 Sr, in good agreement with the microprobe analysis of charoite. The nearest peak from the Sr site (= 2.20 Å) inside the cavity was supposed to be caused by H_2O molecules in site $H_2O(3)$. The occupancy of the $H_2O(3)$ site is 0.36 O (Table 2) and mean bond length $H_2O(3)$–O = 2.87 Å (Table 3). Finally, the remaining cations Ba^{2+}, Mn^{2+} and part of the K^+ were inferred, statistically, to occupy the K(4) site (mean bond length K(4)–O = 2.68 Å) (Tables 2, 3). Thus, H_2O molecules and the impurity cations Sr^{2+}, Ba^{2+}, Mn^{2+} and K^+, which always occur in charoite, are located inside this tube. For the partially occupied positions (especially the Sr position), we can expect ordering along the *z* axis, e.g. alternating 1.0 and 0.0 occupancy for Sr. Such ordering implies a doubling of the *c* parameter and so may be associated with the observed additional rows of weak diffraction maxima halfway between the rows *h*0*l*.

The structure of charoite is unique among alkaline Ca-silicates, in that impurity elements such as Sr, Ba and Mn are abundant; Fe and Ti can also be detected. The various colours of charoite samples depend on the varying amounts of Mn, Fe and Ti; in particular, the colour from light lilac to dark violet depends on the content of Mn^{3+} cations (Evdokimov *et al.*, 2000). In the structures of canasite and frankamenite, these impurity cations were not determined; in the structure of miserite, the rare-earth elements are located in octahedrally-coordinated sites; in the structure of Sr-agrellite, Sr^{2+} substitutes for Ca^{2+} at octahedrally-coordinated sites. In the structure of charoite, all impurity cations are located in the tube formed by the dreier double chain $[Si_6O_{17}]^{10-}$, Ca(5), Ca(6) octahedra and Si(11), Si(12) tetrahedra.

Charge-balance mechanism and crystal chemical formula

The structure of charoite contains 51 O sites (excluding the H_2O molecules). Twenty-nine O atoms make bonds with two Si atoms and their charges are completely compensated. Seven Os have a bond with one Si, and additional bonds with three octahedrally-coordinated cations. Allowing for the occupancy of the Na(1) and Na(2) octahedra by a majority of Na^+ (Table 2), the charges of the corresponding Os are not completely compensated. Twelve O atoms have a bond with one Si atom and additional bonds with two octahedrally-coordinated Ca^{2+} ions. Therefore, we can assume some substitution of O^{2-} by OH^- groups at these O sites. Two O atoms are bonded to one Si and form bonds with one octahedrally-coordinated Ca^{2+} and with cations in the partly occupied Sr and K(4) sites. The anion in the OH forms only three bonds with cations in the Na(1) and Na(2) sites and, thus, it is likely that both OH^- and F^- are located in this position.

From the results of the refinement and charge-balance mechanism the crystal chemical structural formula of charoite can be written as: $(K_{13.88}Sr_{1.0}Ba_{0.32}Mn_{0.36})_{\Sigma 15.56}(Ca_{25.64}Na_{6.36})_{\Sigma 32}[(Si_6(O_{11}(O,OH)_6)_2(Si_{12}(O_{18}(O,OH)_{12})_2(Si_{17}(O_{25}(O,OH)_{18})_2](OH,F)_{4.0}\cdot 3.18H_2O$, $Z = 1$. Taking into account the charge balance, we can formulate $(K_{13.88}Sr_{1.0}Ba_{0.32}Mn_{0.36})_{\Sigma 15.56}(Ca_{25.64}Na_{6.36})_{\Sigma 32}[Si_{70}(O_{170.88}OH_{9.12})_{\Sigma 180}](OH,F)_{4.0}\cdot 3.18H_2O$, or in the general case $(K,Sr,Ba,Mn)_{15-16}(Ca,Na)_{32}[Si_{70}(O,OH)_{180}](OH,F)_{4.0}\cdot nH_2O$.

With $Z = 4$, we obtain $(K_{3.47}Sr_{0.25}Ba_{0.08}Mn_{0.09})_{\Sigma 3.89}(Ca_{6.41}Na_{1.59})_{\Sigma 8}[Si_{17.5}(O_{42.72}OH_{2.28})_{\Sigma 45}](OH,F)_{1.0}\cdot 0.8H_2O$.

In spite of the fact that these data differ from the average result of the microprobe analysis, $(K_{3.28}Sr_{0.26}Ba_{0.08}Mn_{0.09})_{\Sigma 3.71}(Ca_{6.94}Na_{1.37})_{\Sigma 8.31}[Si_{17.65}O_{45}](OH,F)_{1.0}$, the results are well within the limits of the minimum and maximum variations in the chemical composition of the separate analyses. The calculated density based on the results of the structure refinement is 2.55 g cm^{-3} which is in excellent agreement with the measured density of 2.54 g cm^{-3}.

The fact that most of the O sites with (O,OH) are located within the (100) zigzag layers of octahedra suggests that here, only weak bonds are active. As a consequence, the silicate chains connected on opposite sides of the zigzag layers may undergo a cooperative discrete shift of one half of the *z* translation, which corresponds to a stacking fault with fault vector ½[001]. This is a precondition for the occurrence of polytypism. Regular shifts on every layer in the same direction would then result in another species of charoite being monoclinic with $\beta = 96^\circ$ (charoite-96; see also Fig. 4). Shifts alternating on every second layer in the + and − directions respectively, might form the polymorph with a doubled *a* parameter (charoite-2a). Randomly distributed + or − shifts would result in a disordered species (charoite-d).

Summary and discussion

The structure of charoite has been solved by the new method of ADT, coupled with PED. Despite the complex structure of charoite, the large number of reflections collected by ADT (more than 2800 unique reflections) and the strong reduction of dynamic effects enabled us to solve this structure *ab initio* and refine it in a fully automatic way using the same software which has been used for more than forty years in X-ray crystallography. The efficiency and reproducibility of the solution path offered by ADT is a glimpse of a significant step forward in nanostructural investigations. Ongoing improvements for geometric corrections, complete 3D-reconstruction of diffraction patterns and dynamic refinement will, hopefully, lead to a fully automated structure routine for any class of nanomaterials, including organic molecules and other complex inorganic structures, such as zeolites.

The charoite structure is unique in that it consists of three different types of silicate chains; the radical $[Si_{17}(O,OH)_{43}]^{18-}$ builds up a new type of silicate chain – a tubular hybrid dreier quadruple chain (classification after Liebau, 1985).

We have solved the structure of polytype charoite-90 and obtained informations about other polytypes such as charoite-96 and charoite-2a. However, to understand the 'charoite story' more deeply it will be necessary to explore the polytypism in detail and solve the structure of other polytypes.

The polytypic features of charoite may be treated as in other Ca dreier chain silicate minerals (wollastonite, xonotlite, tobermorite *etc.*). In a more formal way, the polytypic features and one-dimensional disorder in charoite may be dealt with through the OD approach. A short account written by Prof. Stefano Merlino is given in the Appendix to this paper.

Acknowledgements

The authors thank the Deutsche Forschungsgemeinschaft for financial support (DE 412/37-1 and SFB 625). They are grateful to T.V. Soboleva (VNIISIMS, Alexandrov) for donating the charoite sample studied in this work, T. Gorelik (Institute of Physical Chemistry, Mainz) for fruitful discussions and software development, Barbara Mader (Institute of Geowissenschaften, Kiel) for the microprobe analysis and Andriy Lotnyk (Technical Faculty, University Kiel) for help at the Technai F30. We thank all referees and M. Welch for their very helpful comments and S. Merlino for his OD approach.

References

Akselrud, L.G., Grin, Yu.N., Zavalii, P.Yu., Pecharsky, V.K. and Fundamensky, V.S. (1989) CSD – the programs for determination and refinement crystal structures. *Collected Abstracts X11 European Crystallography meeting*, *Moscow*, **3**, 155.

Avilov, A., Kuligin, K., Nicolopoulos, S., Nickolskiy, M., Boulahya, K., Portillo, J., Lepeshov, G., Sobolev, B., Collette, J.P., Martin, N., Robins, A.C. and Fischione, P. (2007) Precession technique and electron diffractometry as new tools for crystal structure analysis and chemical bonding determination. *Ultramicroscopy*, **107**, 431–444.

Burla, M.C., Caliandro, R., Camalli, M., Carrozzini, B., Cascarano, G.L., De Caro, L., Giacovazzo, C., Polidori, G., Diligi, S. and Spagna, R. (2007) *IL MILIONE*: a suite of computer programs for crystal structure solution of proteins. *Journal of Applied Crystallography*, **40,** 609–613.

Chiragov, M.I. and Shirinova, A.F. (2004) Crystal structure of charoite; relations to structures of miserite, canasite and okenite. *Mineralogicheskiy Zhurnal*, **26**(4), 5–9. (in Russian).

Czank, M. and Bissert, G. (1993) The crystal structure of $Li_2Mg_2[Si_4O_{11}]$, a loop-branched dreier single chain silicate. *Zeitschrift für Kristallographie*, **204**, 129–142.

Evdokimov, M.D., Bulach, À.G. and Borisov, À.B. (1995) Morphogenetic types of charoite and their jeweller's qualities. *Mineralogicheskiy Zhurnal*, **7**(5), 24–31. (in Russian).

Evdokimov, M.D., Rodishevskii, D.V. and Fadeeva, I.K. (2000) About the tints of charoite colourings. *Abstracts of Meeting "Mineralogical Museums"*, St.Petersburg, 42–43. (in Russian).

Frank-Kamenetskaya, O.V. and Rozhdestvenskaya, I.V. (2004) *Atomic defects and crystal structure of minerals*. St.Petersburg, Yanus, Crystal Chemistry, **33,** 187 pp.

Heil, U., Schlitt, S. and Schömer, E. (2009) *ADT-3D – a software package for ADT data visualizing and processing, which improves and extends existing Matlab applications especially about 3D algorithms.* Institute of Computer Science, Johannes Gutenberg-University of Mainz, Germany.

Kolb, U., Gorelik, T., Kübel, C., Otten, M.T. and Hubert, D. (2007) Towards automated diffraction tomography: Part I – Data acquisition. *Ultramicroscopy*, **107**, 507–513.

Kolb, U., Gorelik, T. and Otten, M.T. (2008) Towards automated diffraction tomography. Part II - Cell parameter determination. *Ultramicroscopy*, **108**, 763–772.

Konev, A.A., Vorob'ev, E.I. and Lazebnik, K.A. (1996) *Mineralogy of Murunskii Alkaline Massif*. Nauchno-Izdatelsky Tsentr Ob'edinennogo Instituta Geologii, Geofiziki, Mineralogii, Siberian Branch of Russian Academy of Science, Novosibirsk, Russia, 221 pp. (in Russian).

Liebau, F. (1985) *Structural Chemistry of Silicates*. Springer-Verlag, Berlin, Heidelberg, 412 pp.

Mugnaioli, E., Gorelik, T. and Kolb, U. (2009) 'Ab initio' structure solution from electron diffraction data obtained by a combination of Automated Diffraction Tomography and Precession Technique. *Ultramicroscopy*, **109**, 758–765.

NanoMEGAS (2004) *Advanced Tools for Electron Diffraction*. Available at <http://www.nanomegas.com>.

Nikishova, L.V., Lazebnik, K.A. and Lazebnik, Yu.D. (1985) About crystallochemical formulae of charoite. Pp. 100–105 in: *Crystal Chemistry and Structure of Minerals*. Nauka, Leningrad, Russia. (in Russian).

Own, C.S. (2005) *System design and verification of the precession electron diffraction technique*. Ph.D. thesis, Northwestern University, Evanston, Illinois, USA. Available at <http://www.numis.northwestern.edu/Research/Current/precession>.

Rogova, V.P., Rogov, Yu.P., Drits, V.A. and Kuznetsova, N.N. (1978) Charoite – a new mineral and a new jewelry stone. *Zapiski Vsesoyuznogo Mineralogicheskogo Obshchestva*, **107**, 94–100. (in Russian).

Rozhdestvenskaya, I.V. and Nikishova, L.V. (2002) Characteristics of Alkali Calcium Silicates from Charoitites. *Crystallography Reports*, **47**, 545–554.

Rozhdestvenskaya, I.V., Kogure, T. and Drits, V.A. (2007) Structural model of charoite. *Abstracts of Meeting "Crystal chemistry and X-ray diffraction of Minerals"*. Miass, Russia, 48–49.

Rozhdestvenskaya, I.V., Kogure, T. and Drits, V.A. (2009*a*) Structural model of charoite. *Mineralogical*

Magazine, **73**, 883–890.

Rozhdestvenskaya, I., Kolb, U., Mugnaioli, E., Reinholdt, A., Weirich, T., Depmeier, W. and Czank, M. (2009*b*) Some news about charoite. *Zeitschrift für Kristallographie*, Supplement Issue, **29**, 103.

Sheldrick, G.M. (1997) *SHELXL97. Program for the Refinement of Crystals Structures*. University of Göttingen, Göttingen, Germany.

Sheldrick, G.M. (2008) A short history of SHELX. *Acta Crystallographica A*, **64**, 112–122.

Vincent, R. and Midgley, P.A. (1994) Double conical beam-rocking system for measurement of integrated electron diffraction intensities. *Ultramicroscopy*, **53**, 271–282.

Vorob'ev, E.I. (2008) *Charoite* (L.D. Zorina, editor). Academy Publishing 'Geo', Novosibirsk, Russia, 140 pp. (in Russian).

APPENDIX

A short account of an OD approach to polytypism in charoite

Stefano Merlino, Dipartimento di Scienze della Terra, via S. Maria 53, I-56126 Pisa, Italy

Charoite consists of OD layers with translation vectors **b** and **c** (with a third basic vector $\mathbf{a}_0$, with $a_0 = a/2$) and layer group symmetry $P(2)mm$ (λ-POs, partial operations of the layer; the parentheses in the second position of the symbol indicate the direction of missing periodicity). The OD theory has derived the possible sets of operations converting a layer into the succeeding one (σ-POs) compatible with the 80 groups of layer symmetry. In the present case they are indicated in the following:

P	(2)	m	m	
	$\{(n_{1,1/2})$	2_1	$2_{1/2}\}$	σ-POs converting the first layer into the second
	$\{(n_{1,1/2})$	2_1	$2_{1/2}\}$	σ-POs converting the second layer into the third

(three lines are necessary here as the present OD family belongs to the third category of OD structures built up by equivalent layers).

We focus our attention on the σ-POs $2_{1/2} \parallel \mathbf{c}$, namely rotation by 180º, followed by translation of **c**/4; their position is indicated in Fig. A1. Due to the mirror plane normal to **c**, operations $2_{1/2}$ and $2_{-1/2}$ give rise to geometrically equivalent pairs of adjacent layers.

An infinite number of possible ordered (polytypes) or disordered sequences of layers is possible, corresponding to the infinite sequences of $2_{1/2}$ and $2_{-1/2}$ operations relating adjacent layers. The OD theory singles out a few sequences (two in the present case) with a maximum degree of order, the 'MDO structures', corresponding to the polytypes with homogeneous sequences of layers in Zvyagin's terminology.

MDO1: $2_{-1/2}$, $2_{1/2}$, $2_{-1/2}$, $2_{1/2}$ ·····. In the first MDO polytype, $2_{1/2}$ and $2_{-1/2}$ operations alternate regularly. The mirror plane normal to **c** is lost, as well as the twofold axis ∥ **a**. Valid operations for the whole structure are the λ-POs *m* normal to **b**, the σ-PO $2_1 \parallel \mathbf{b}$ and the σ-POs inversion centres located on these axes.

The basic translations of the structure are: $\mathbf{a} = 2\mathbf{a}_0$, **b**, **c**, with parameters $a = 31.96$, $b = 19.64$, $c = 7.09$ Å, $\beta = 90º$, space group $P2_1/m$.

MDO2: $2_{-1/2}$, $2_{-1/2}$, $2_{-1/2}$, $2_{-1/2}$ ·····. In the second MDO polytype, $2_{-1/2}$ operations are applied constantly: the constant application of $2_{1/2}$ operation gives rise to the same structure in twin relationships, twin plane (100). Also, in this

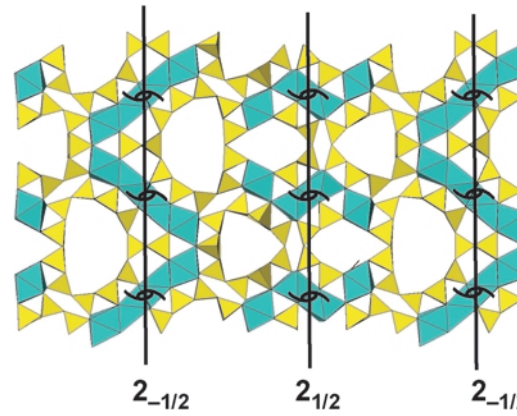

FIG. A1. The structure of the tetrahedral-octahedral framework of charoite (MDO1 polytype) as seen down [001], **a** horizontal. The vertical lines indicate the approximate borders between successive OD layers, which have layer symmetry $P2mm$. The first vertical row of $2_{-1/2}$ operations is followed by a vertical row of $2_{1/2}$ operations, and by another vertical row (last, at right) of $2_{-1/2}$ operations.

case the mirror plane normal to **c** is lost, as well as the twofold axis || **a,** and valid operations for the whole structure are the λ-POs *m* normal to **b**, and the two σ-POs 2_1 || **b** and inversion centres.

The basic translations of the structure are: **a** = $2\mathbf{a}_0$ + **c**/2, **b**, **c**, with parameters a = 32.16, b = 19.64, c = 7.09 Å, β = 96.33º, space group $P2_1/m$ (the parameters correspond to those given by Rozhdestvenskaya *et al*., 2007, 2009*a*).

It is remarkable that all the polytypes, as well as the disordered sequences, should present a common set of reflections, those with $l = 2n$. This set of reflections, the so-called 'family reflections', is always sharp, and in case of disordered sequences should display orthorhombic symmetry. The various polytypes give rise to distinct diffraction patterns for $l = 2n+1$, with continuous streaks for the disordered sequences.